déduit que (Tableau 5) le calcium donne environ 0,33 u.v.e. à l'atome de chlore des sites Cl(1) et environ 0,62 u.v.e. à l'atome de chlore des sites Cl(2). Comme Cl(2) est à peu près à la même distance de Ca que Cl(1), il reçoit de cet atome Ca environ 0,33 u.v.e.; le complément à 0,62 u.v.e. fourni par le calcium, c'est-à-dire 0,29 u.v.e., ne peut alors provenir que de Ca^{I} situé à 2,933 Å. L'ion chlore Cl(2) appartient donc au polyèdre de coordination de deux atomes de calcium, constitué d'un prisme droit à base triangulaire dont l'une des faces rectangulaire est surmontée d'une pyramide (Fig. 1). Cette forme de polyèdre a aussi été observé dans $Ca(C_4H_3O_4)_2.5H_2O$ étudié par Hsu & Schlemper (1978).

L'atome de calcium est alors entouré de trois ions chlore et quatre molécules d'eau qui conduisent à une coordinence de sept et non de six comme le proposèrent Thewalt & Bugg (1973). On peut, par conséquent, décrire la structure comme formée de dimères centrosymétriques $[CaCl_2.4H_2O]_2$, dans lesquels les deux ions calcium sont pontés par deux ions chlore (Fig. 2). La cohésion entre eux est assurée par des liaisons hydrogène principalement entre l'eau et le chlore (Tableau 4).

Références

BROWN, I. D. (1976*a*). *Acta Cryst.* A**32**, 24–31.

BROWN, I. D. (1976*b*). *Acta Cryst.* A**32**, 786–792.

BROWN, I. D. & WU, K. K. (1976). *Acta Cryst.* B**32**, 1957–1959.

CROMER, D. T. (1965). *Acta Cryst.* **18**, 17–23.

CROMER, D. T. & WABER, J. T. (1965). *Acta Cryst.* **18**, 104–109.

FERRARIS, G. & FRANCHINI-ANGELA, M. (1972). *Acta Cryst.* B**28**, 3572–3583.

HSU, B. & SCHLEMPER, E. O. (1978). *Acta Cryst.* B**34**, 930–932.

LECLAIRE, A. & BOREL, M. M. (1977). *Acta Cryst.* B**33**, 1608–1610.

LECLAIRE, A. & MONIER, J. C. (1977). *Acta Cryst.* B**33**, 1861–1866.

PAULING, L. (1929). *J. Am. Chem. Soc.* **51**, 1010–1026.

THEWALT, U. & BUGG, C. E. (1973). *Acta Cryst.* B**29**, 615–617.

Acta Cryst. (1979). B**35**, 588–592

Refinement of the Crystal Structure of Terbium Arsenate $TbAsO_4$ at 77 K and 5 K by Profile Analysis from Neutron Diffraction Powder Data

BY W. SCHÄFER AND G. WILL

Mineralogisches Institut der Universität Bonn, Lehrstuhl für Mineralogie und Kristallographie, 5300 *Bonn, Federal Republic of Germany*

AND G. MÜLLER-VOGT

Kristall- und Materiallabor der Fakultät für Physik, Universität Karlsruhe, 7500 *Karlsruhe, Federal Republic of Germany*

(*Received* 31 *August* 1978; *accepted* 8 *December* 1978)

Abstract

Terbium arsenate $TbAsO_4$ undergoes a crystallographic phase transition at T_d = 27·7 K from tetragonal ($I4_1/amd$) to orthorhombic symmetry ($Fddd$). The lattice parameters are a = 7·090 (3) and c = 6·320 (3) Å above and a = 10·081 (3), b = 9·957 (3), and c = 6·321 (2) Å below T_d. Least-squares refinements of the atomic positions from neutron diffraction powder intensities taken at 77 and 4·2 K led to R values of 5·6 and 4·7% respectively. The phase transition affects the interatomic distances between the Tb ions and is thus of importance in the magnetic behavior of $TbAsO_4$.

0567-7408/79/030588-05$01.00

Introduction

The heavy rare-earth vanadates and arsenates, $LnVO_4$ and $LnAsO_4$, are characterized by a crystallographic phase transition at temperatures T_d followed by a second phase transition to an antiferromagnetically ordered state at the Néel temperatures T_N. T_d is always well above the Néel temperature T_N (Will, Schäfer, Scharenberg & Göbel, 1971). The crystallographic phase transitions are generally attributed to a cooperative Jahn–Teller distortion (Cooke, Ellis, Gehring, Martin, Wanklyn, Wells & White, 1970).

The compounds crystallize at room temperature with the tetragonal zircon-type structure, space group

$I4_1/amd$. At temperatures T_d a reduction to orthorhombic symmetry has been observed in the terbium and dysprosium vanadates and arsenates (Göbel & Will, 1972; Will, Göbel, Sampson & Forsyth, 1972). The transitions were studied by X-ray diffraction on powders and limited to the unit-cell distortions.

In this paper we report on a neutron diffraction study of $TbAsO_4$. With neutrons the rare-earth ions are not considered heavy in comparison to oxygen, as is the case for X-rays, and the least-squares refinement can be extended to the crystal structure, including the atomic positions.

Specific-heat measurements on $TbAsO_4$ have shown a triangular-shaped anomaly at $T_d = 27{\cdot}7$ K and a λ-type anomaly at $T_N = 1{\cdot}5$ K (Berkhahn, Kahle, Klein & Schopper, 1973). From spectroscopic measurements the former was attributed to a crystallographic phase transition to lower symmetry, while the latter represents the antiferromagnetic phase transition (Wüchner, Böhm, Kahle, Kasten & Laugsch, 1972). The reduction in symmetry at T_d could be confirmed by X-ray diffraction, where a centroidal splitting of the tetragonal *hhl* reflections was observed below T_d = 27 K. Orthorhombic symmetry was assumed below 27 K and the space group *Fddd* was proposed (Göbel, Müller-Vogt, Orlich & Klein, 1972).

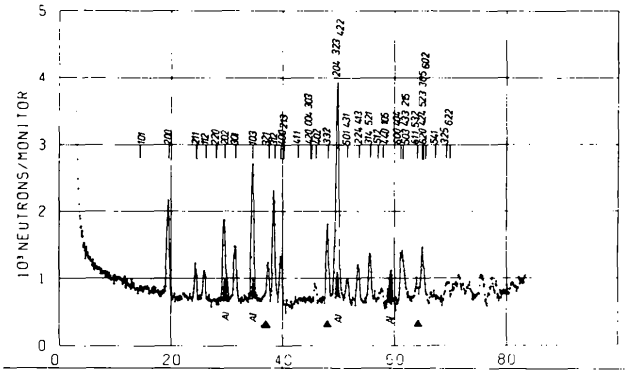

(*a*)

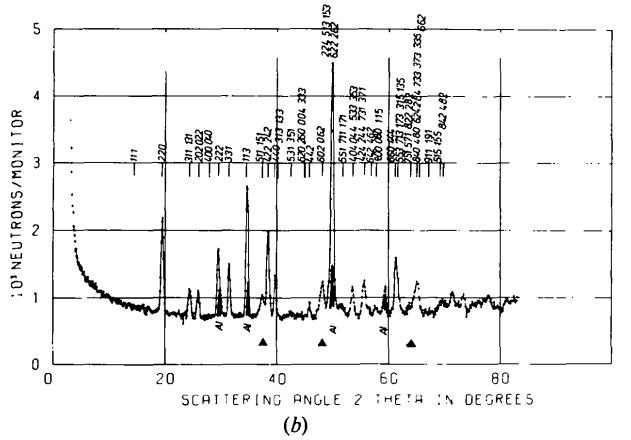

(*b*)

Fig. 1. Neutron diffraction diagrams of $TbAsO_4$ at (*a*) 77 K and (*b*) 4·2 K. Peak broadenings due to the crystallographic phase transition at 27·7 K are indicated by arrows.

Experimental

The powder was ground from crystals grown by a flux method (Hintzmann & Müller-Vogt, 1969) and housed in an aluminium container of diameter 7 mm and height 30 mm. The neutron diffraction diagrams were measured at three temperatures, 300, 77 and 5 K. The diagrams were measured in steps of 0·1° using 1·203 Å neutrons and the diffractometer KATINKA of the University of Bonn at the DIDO research reactor, Kernforschungsanlage Jülich. The diagrams taken at 77 and 5 K are shown in Fig. 1.

Structure refinement

Using the data collected at 77 K, lattice parameters and positional parameters x(O) and z(O) (Table 1) were refined simultaneously by least-squares methods based on profile analysis (Rietveld, 1969). Additional least-squares calculations were performed for refinement of the atomic positions only, by our program *POWLS* which uses the total integrated intensities of individual peaks or groups of overlapping peaks in the least-squares calculation (Schäfer & Will, 1976). Both procedures resulted in the same parameters, as listed in Table 1. The neutron-scattering lengths used were b_{Tb} = 0·76, b_{As} = 0·64 and b_O = 0·5803 ($\times 10^{-11}$ mm) (Bacon, 1972). With 22 powder peaks containing 36 reflections *POWLS* led to $R = 0{\cdot}056$ with $R = (\sum |I_o - I_c|)/\sum I_o$.*

* Tables of the observed neutron intensities together with the calculated values from both refinement methods for the 77 and 5 K data have been deposited with the British Library Lending Division as Supplementary Publication No. SUP 34146 (3 pp.). Copies may be obtained through The Executive Secretary, International Union of Crystallography, 5 Abbey Square, Chester CH1 2HU, England.

Table 1. *Structural data of* $TbAsO_4$ *above and below the crystallographic phase transition at* $T_d = 27{\cdot}7$ K

Standard deviations are given in parentheses.

	$T = 77$ K	$T = 5$ K
Space group	$I4_1/amd$	*Fddd*
a (Å)	7·090 (3)	10·081 (3)
b (Å)		9·957 (3)
c (Å)	6·320 (3)	6·321 (2)
V (Å^3)	317·71 (21)	634·52 (40)
Z	4	8
Tb sites (*a*)	000	000
As sites (*b*)	$00\frac{1}{2}$	$00\frac{1}{2}$
O sites (*h*)	0*xz*	*xyz*
x(O)	0·181 (1)	0·090 (1)
y(O)		0·089 (1)
z(O)	0·330 (1)	0·331 (1)
D_x (Mg m^{-3})	6·295	6·304

In the diffraction pattern taken at 5 K significant broadenings can be observed at some peaks with the general indices *hhl*, indicated by arrows in Fig. 1. As an example we have depicted in Fig. 2 the tetragonally degenerate 332 peak near $2\theta = 48°$ for 77 and 5 K on an expanded scale. The half-width increases from $\Delta(2\theta) = 0{\cdot}48$ to $0{\cdot}95°$. We have employed a further profile analysis of this peak using a least-squares fit with overlapping Gaussian peaks of normal half-widths. The result is shown in Fig. 3. Variables were the two positions and the peak heights, indicating the intensity. The result is two Gaussian curves of nearly equal intensity centered at $2\theta = 47{\cdot}75 \pm 0{\cdot}02°$ and $48{\cdot}23 \pm 0{\cdot}02°$.

Splitting of the degenerate *hhl* reflections means the loss of tetragonal symmetry and reduction to orthorhombic symmetry. The full analysis of the whole diagram leads to a distortion similar to that observed earlier in $TbVO_4$ (Will, Göbel, Sampson & Forsyth, 1972): the distortion of the unit cell occurs along the face diagonals [110] and [$\bar{1}$10] ($a_{orth} \simeq \sqrt{2}a_{tetr}$ and $b_{orth} \simeq \sqrt{2}a_{tetr}$), while the c axis is unaffected (Fig. 4). The

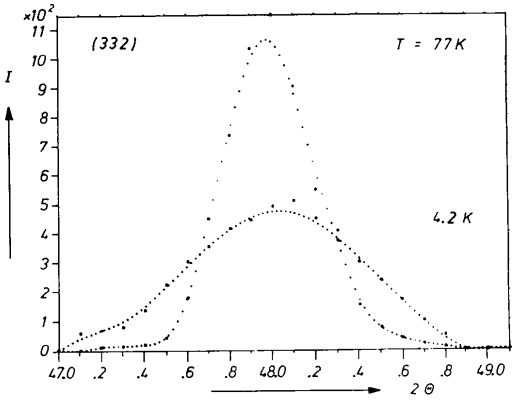

Fig. 2. Increase of the half-width of the tetragonal 332 peak from 0·48° at 77 K to 0·95° in the orthorhombic phase at 5 K. Measured points are shown as filled squares, calculated points are crosses.

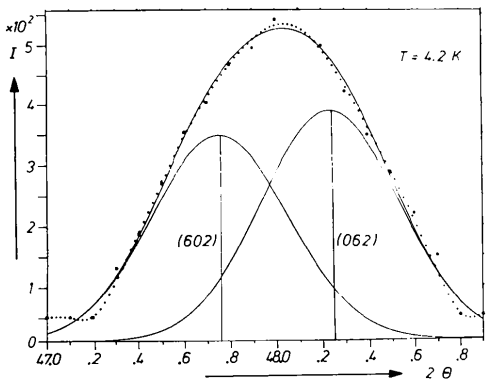

Fig. 3. Gaussian peak profile analysis of the broadened tetragonal 332 peak resulting in two Gaussian peaks of normal half-width which represent the orthorhombic 602 and 062 peaks.

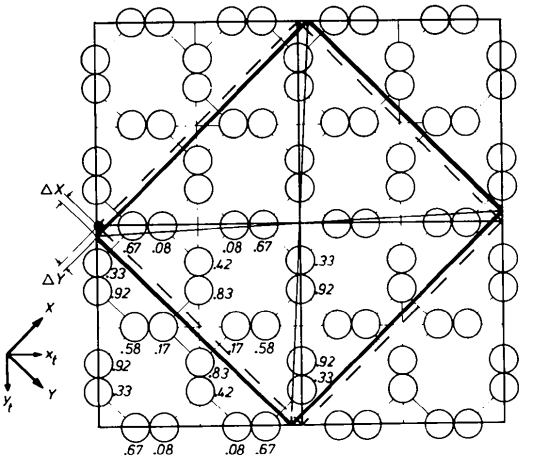

Fig. 4. $X-Y$ projection of the tetragonal and orthorhombic lattices of $TbAsO_4$ showing the crystallographic distortion along the face diagonals with $\Delta X = -\Delta Y$. The circles represent the O atoms with the z parameters common to both phases.

orthorhombic space group is *Fddd*, a proper equitranslational subgroup of $I4_1/amd$ and therefore in agreement with this transition. The ensuing least-squares calculation, again by both methods, led to the new lattice parameters and also to the new positional parameters listed in Table 1. With 19 powder peaks containing 36 reflections *POWLS* led to $R = 0{\cdot}047$. Again both least-squares methods, one based on profile analysis and the other based on integrated intensities, yielded the same results. It is worth mentioning that the refinement of the lattice parameters with Rietveld's program yielded the values $2\theta = 47{\cdot}75 \pm 0{\cdot}03°$ and $48{\cdot}24 \pm 0{\cdot}03°$ for the orthorhombic 602 and 062 reflections respectively, which is in full agreement with the independent Gauss analysis of the corresponding broadened 332 peak of Fig. 3.

Discussion of the transformation

As with other compounds of this series studied previously ($TbVO_4$, $DyVO_4$ and $DyAsO_4$) the crystallographic phase transition at 27·7 K occurs, within error limits, without a detectable change of the unit-cell volume: $V_{orth} \simeq 2V_{tetr}$ (see Table 1). The fractional changes of a and b, with $\Delta a \simeq -\Delta b$, are $12{\cdot}4 \times 10^{-3}$ Å for $TbAsO_4$, which is significantly lower than those in $TbVO_4$ of $21{\cdot}7 \times 10^{-3}$ Å. The corresponding values for the dysprosium compounds with distortions along [100] and [010] (space group *Imma*) are $4{\cdot}2 \times 10^{-3}$ Å for $DyAsO_4$ and $4{\cdot}8 \times 10^{-3}$ Å for $DyVO_4$.

In the terbium compounds we observe a distortion of the angle between the tetragonal face diagonals of about 1°, and consequently the resulting interatomic displacements of the ions during the crystallographic

phase transition are small. Table 2 lists distances and angles for both phases. The calculated changes in the AsO_4 tetrahedra are about 0·03 Å and 1°, which equal the error limits. Likewise no changes in the Tb–O distances are detectable.

For an understanding of the phase transition we must discuss the configurations around the As and Tb ions in the crystal structure of $TbAsO_4$. An essential structural element is the AsO_4 tetrahedron. The O^{i} and O^{ii} atoms in Fig. 5 are of special interest. They form the corners of the AsO_4 tetrahedron oriented along [1̄10] and they are coupled directly to the magnetic Tb ions.

Table 2. *Atomic distances* (Å) *and angles* (°) *in* $TbAsO_4$ *at* 77 K *and* 5 K (*see Fig.* 5)

Standard deviations are given in parentheses.

	$T = 77$ K	$T = 5$ K
AsO_4 tetrahedron		
As–$O^{i(ii,iii,iv)}$	1·67 (1)	1·66 (1)
$O^{i(iii)}$–$O^{ii(iv)}$	2·57 (1)	2·54 (3)
$O^{i(ii)}$–$O^{iii(iv)}$	2·81 (1)	2·80 (1)
$O^{i(ii)}$–$O^{iv(iii)}$	2·81 (1)	2·78 (2)
$O^{i(iii)}$–As–$O^{ii(iv)}$	100·1 (6)	99·8 (9)
$O^{i(ii)}$–As–$O^{iii(iv)}$	114·3 (3)	115·4 (6)
$O^{i(ii)}$–As–$O^{iv(iii)}$	114·3 (3)	113·7 (9)
Tb environment		
Tb–$O^{v(vi,vii,viii)}$	2·32 (1)	2·33 (1)
Tb–$O^{i(ii,iii',iv')}$	2·45 (1)	2·45 (1)
$O^{v(vii)}$–Tb–$O^{vi(viii)}$	154·8 (6)	154·6 (9)
Magnetically relevant Tb distances		
Tb–Tb (4×)	3·881 (2)	3·879 (1)
Tb–Tb (4×)	5·919 (3)	5·918 (1)
Tb–Tb (8×)	5·926 (3)	5·897 (2) 5·949 (2)

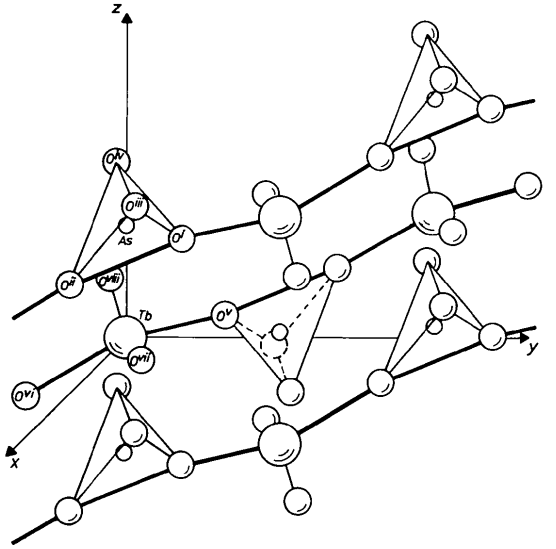

Fig. 5. Arrangement of AsO_4 tetrahedra in a chain with Tb. As is tetrahedrally surrounded by O atoms. Three chains of –O–O–Tb–O–O along [1̄10], which transmit the long-range interaction for the crystallographic distortion, are shown.

We believe that these chains –O–O–Tb–O–O–Tb– oriented along [110] {and [1̄10]} and parallel to the direction of the observed crystallographic distortion are the essential elements for the Jahn–Teller distortion and also for the magnetic interaction.

While the crystallographic phase transition is of no consequence for the O ions (coordination and distances) it affects the interatomic distances between the Tb ions, which are finally responsible for the magnetic structure. The Tb ion at the body center $\frac{1}{2},\frac{1}{2},\frac{1}{2}$ is surrounded by four nearest Tb neighbors at the corners of a tetrahedron at distances of 3·881 Å (Table 2). Looking at the next-nearest neighbors (at 5·9 Å), we have 12 next-nearest Tb ions above $T_d = 27{\cdot}7$ K, namely four Tb ions at the corners of a second regular tetrahedron at distances of 5·919 Å, which is penetrated by an equidistant group of eight next-nearest Tb neighbors 5·926 Å away at the corners of the original tetragonal unit cell, *i.e.* at the corners of a tetragonal prism, $c/a = 0{\cdot}89$. This second group of next-nearest Tb neighbors, and only this group, is affected by the crystallographic phase transition. The lattice distortion is fully translated to these atoms and leads to a significant splitting of these eight Tb neighbors into two groups, leading to differences of 0·06 Å in the distances to the central Tb ion (the standard deviation is 0·002 Å).

The observed long-range effect of the phase transition corroborates the conclusions from spectroscopic measurements (Wüchner, Böhm, Kahle, Kasten & Laugsch, 1972) that the crystallographic phase transition in $TbAsO_4$ at 27·7 K occurs very similarly to those observed in $DyVO_4$ at 13·8 K, $DyAsO_4$ at 11·2 K, and $TbVO_4$ at 33·0 K. (For these crystals no information on the crystal structure is available.) According to Elliott, Harley, Hayes & Smith (1972) the crystallographic phase transition in these latter compounds can be understood by a cooperative Jahn–Teller effect with dominant long-range interactions. The theoretical understanding of the transition is in principle based on a molecular-field treatment, in the earlier theories (Öpic & Pryce, 1957) using single-ion theory only, later also including strain coupling (Kanamori, 1960). The rare-earth ions are coupled to the optic phonon modes, *i.e.* the interaction between the rare-earth sites is conveyed *via* the phonons and one obtains coupled spin-phonon modes, which are familiar, for example, in hydrogen-bonded ferroelectrics.

It is in this connection that we place special significance on the chains ...–O–O–Tb–O–O–... along orthorhombic [110] and [1̄10], *i.e.* along the O–O bonds of the AsO_4 tetrahedron bonded to Tb. There is a network of such chains running crosswise along [110] and [1̄10] through the crystal. Three such chains are depicted in Fig. 5. The observed distortion of the unit cell and the measured changes only in the next-nearest Tb–Tb distances can thus be understood.

In these rare-earth systems studied here and previously, the soft mode which causes the phase transition to occur is electronic, and arises because there is an effective quadrupolar coupling between the rare-earth ions. This quadrupolar coupling has already been postulated in an earlier investigation (Will & Schäfer, 1971) and treated theoretically by Sivardière & Blume (1972).

This work has received the support of the Bundesministerium für Forschung und Technologie, Bonn, which is gratefully acknowledged.

References

BACON, G. E. (1972). *Acta Cryst.* A**28**, 357–358.

BERKHAHN, W., KAHLE, H. G., KLEIN, L. & SCHOPPER, H. C. (1973). *Phys. Status Solidi B*, **55**, 265–271.

COOKE, A. H., ELLIS, C. J., GEHRING, K. A., MARTIN, D. M., WANKLYN, B. H., WELLS, M. R. & WHITE, R. L. (1970). *Solid State Commun.* **8**, 689–692.

ELLIOTT, R. J., HARLEY, R. T., HAYES, L. & SMITH, S. R. P. (1972). *Proc. R. Soc. London Ser. A*, **328**, 217–266.

GÖBEL, H., MÜLLER-VOGT, G., ORLICH, L. & KLEIN, L. (1972). *Phys. Lett. A*, **41**, 409–410.

GÖBEL, H. & WILL, G. (1972). *Phys. Status Solidi B*, **50**, 147–154.

HINTZMANN, W. & MÜLLER-VOGT, G. (1969). *J. Cryst. Growth*, **5**, 274–278.

KANAMORI, J. (1960). *J. Appl. Phys.* **31**, 14S–23S.

ÖPIC, U. & PRYCE, M. H. L. (1957). *Proc. R. Soc. London Ser. A*, **238**, 425–447.

RIETVELD, H. M. (1969). *J. Appl. Cryst.* **2**, 65–71.

SCHÄFER, W. & WILL, G. (1976). *Z. Kristallogr.* **144**, 217–225.

SIVARDIÈRE, J. & BLUME, M. (1972). *Phys. Rev. B*, **5**, 1126–1134.

WILL, G., GÖBEL, H., SAMPSON, C. F. & FORSYTH, J. B. (1972). *Phys. Lett. A*, **38**, 207–208.

WILL, G. & SCHÄFER, W. (1971). *J. Phys. C*, **4**, 811–819.

WILL, G., SCHÄFER, W., SCHARENBERG, W. & GÖBEL, H. (1971). *Z. Angew. Phys.* **32**, 122–127.

WÜCHNER, W., BÖHM, W., KAHLE, H. G., KASTEN, A. & LAUGSCH, J. (1972). *Phys. Status Solidi B*, **54**, 273–283.

Acta Cryst. (1979). B**35**, 592–596

Organometallic Compounds Containing a Guanidinium Group. Crystal and Molecular Structure of (Creatinine)phenylmercury(II) Nitrate Monohydrate

BY ALLAN J. CANTY,* NARONGSAK CHAICHIT AND BRYAN M. GATEHOUSE

Chemistry Department, Monash University, Clayton, Victoria 3168, *Australia*

(*Received* 19 *September* 1978; *accepted* 1 *November* 1978)

Abstract

$[Hg(C_6H_5)(C_4H_7N_3O)].NO_3.H_2O$, $C_{10}H_{12}HgN_4O_4.H_2O$ is monoclinic with $a = 10{\cdot}255\,(5)$, $b = 19{\cdot}838\,(9)$, $c = 6{\cdot}859\,(3)$ Å, $\beta = 97{\cdot}81\,(10)°$, $Z = 4$, space group $P2_1/n$. The structure was refined to $R = 0{\cdot}071$. The complex has a $PhHg^{II}$ group bonded to a ring N atom of creatinine to form the cation $[PhHgNC(NH_2)N(Me)CH_2CO]^+$. The C–Hg–N group is non-linear, 174 (1)°, and there is a weak interaction between Hg and a nitrate O atom. The creatinine and phenyl rings are almost coplanar, and the cations are stacked approximately along [001] with phenyl and creatinine rings of adjacent ions almost parallel and 3·372 Å apart.

Introduction

Basic phenylmercuric nitrate, $PhHg(OH.NO_3)_{1/2}$, reacts with creatinine (I) in aqueous ethanol to form a 2:1 complex $[(PhHg)_2C_4H_6N_3O][NO_3]$ which exists in two crystalline forms, and in the presence of nitric acid a 1:1 complex containing the cation $[PhHg(C_4H_7N_3O)]^+$ is formed (Canty, Fyfe & Gatehouse, 1978). ^1H NMR spectra of the complexes and creatinine hydronitrate (II), and a crystal structure determination of one crystalline form of the 2:1 complex (III), indicate that they contain a planar guanidinium group based on $[CN_3]^+$.

Infrared spectra of the complexes and their deuterated analogues are consistent with bonding of $PhHg^{II}$ to the exocyclic N atom in the 1:1 complex (IV), although the alternative structure (V) could not be eliminated. In order to determine whether (IV) or (V) exists in the solid state we have determined the structure of $[PhHg(C_4H_7N_3O)][NO_3].H_2O$.

* Present address: Chemistry Department, University of Tasmania, Hobart, Tasmania 7001, Australia.

0567-7408/79/030592-05$01.00